Supplementary Materials
Stacking-switching of silicon-based two-dimensional diamane structures to enhance photocatalytic water splitting performance

Min Tao,[a,†] Chu-Chu Liu,[a,†] Pan Ma,[a] Xiao Shang,[a] Hai-Bin Du,[b] Xian-Yu Hu,[c] Lu-Chao Du,*[a] Fu-Chun Liu,*[a]

[a] *Institute of Atomic and Molecular Physics, Jilin University, Changchun 130012, China*
[b] *Liaoning Advertising Vocational College, Shenyang 110148,China*
[c] *School of Mechanical and Energy Engineering, Beijing University of Technology, Peking 100124, China*

Author to whom correspondence should be addressed: lcdu@jlu.edu.cn **and** lfc@jlu.edu.cn

†These authors contributed equally to this work.

We calculated the bond orders of Si_4HX monolayers using the Density Derived Electrostatic and Chemical 6th-generation (DDEC6) atomic population analysis method.[1] Bond order is defined as half the difference between the number of bonding electrons and antibonding electrons between two atoms. A larger bond order indicates a stronger bond strength between the same atomic components. As observed in Table S1, the bond order value between the Si4 and *X* atoms in the Si_4HX monolayers is the largest, suggesting that the strongest bond strength between them. In addition, the bond orders of the corresponding atomic bonds in the initial and final states of the Si_4HX monolayers remain nearly unchanged, indicating that this kind of structural transformation does not affect the atomic bond strengths within these structures, which also facilitates the transition between the initial and final states of the Si_4HX monolayers.

Table S1 The DDEC6 bond orders between each pair of atoms in Si_4HX monolayers.

Material	H-Si1	Si1-Si2	Si2-Si3	Si3-Si4	Si4-*X*
Si_4HF_{IS}	0.9138	0.8776	0.8896	0.8584	1.1956
Si_4HF_{FS}	0.9150	0.8792	0.8651	0.8610	1.2014
Si_4HCl_{IS}	0.9139	0.8793	0.8807	0.8546	1.1852
Si_4HCl_{FS}	0.9140	0.8809	0.8572	0.8574	1.1900
Si_4HBr_{IS}	0.9150	0.8760	0.8778	0.8560	1.1036
Si_4HBr_{FS}	0.9152	0.8781	0.8539	0.8585	1.1088

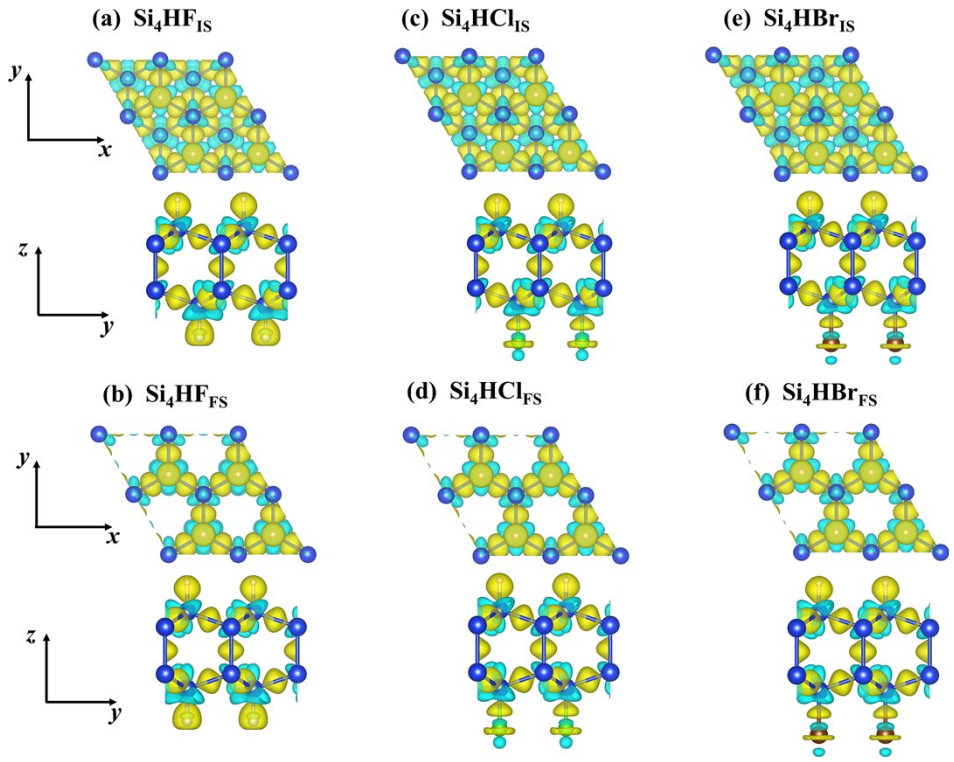

Fig. S1 Three-dimensional charge density difference of the Si_4HX monolayers. The yellow and blue areas represent the accumulation and depletion of electrons with 0.001 eV/ Å^3 iso-surfaces, respectively.

Table S2 The conduction band minimum (CBM) ,valence band maximum (VBM) and bandgap *E*g under different calculation methods of the Si_4HX monolayers (in units of eV).

Monolayer	method	VBM	CBM	E_g
Si_4HF_{IS}	PBE	-3.34	-2.10	1.24
	HSE	-3.89	-1.97	1.92
	G0W0	-2.58	-0.58	2.00
Si_4HF_{FS}	PBE	-3.12	-2.08	1.04
	HSE	-3.66	-1.94	1.72
	G0W0	-3.10	-0.83	2.27
Si_4HCl_{IS}	PBE	-2.56	-1.29	1.27
	HSE	-2.98	-1.05	1.93
	G0W0	-2.63	-0.24	2.39
Si_4HCl_{FS}	PBE	-2.44	-1.38	1.06
	HSE	-2.91	-1.19	1.72
	G0W0	-2.48	-0.29	2.19
Si_4HBr_{IS}	PBE	-2.36	-1.17	1.19
	HSE	-2.84	-0.97	1.87
	G0W0	-2.46	-0.16	2.30
Si_4HBr_{FS}	PBE	-2.19	-1.19	1.00
	HSE	-2.70	-1.04	1.66
	G0W0	-2.28	-0.19	2.10

The solar-to-hydrogen (STH) efficiency η_{STH} is calculated by: [2]

$$\eta_{STH} = \eta_{abs} \times \eta_{cu} \tag{S1}$$

where η_{abs} and η_{cu} represent the light absorption efficiency and carrier utilization efficiency, respectively, given by:

$$\eta_{abs} = \frac{\int_{E_g}^{\infty} P(\mathrm{h}\omega) d(\mathrm{h}\omega)}{\int_{0}^{\infty} P(\mathrm{h}\omega) d(\mathrm{h}\omega)} \tag{S2}$$

$$\eta_{cu} = \frac{\Delta G \int_{E}^{\infty} \frac{P(\mathrm{h}\omega)}{\mathrm{h}\omega} d(\mathrm{h}\omega)}{\int_{E_g}^{\infty} P(\mathrm{h}\omega) d(\mathrm{h}\omega)} \tag{S3}$$

Here, $P(\hbar w)$ is the AM1.5G solar energy flux with the photon energy. E_g and ΔG signify the direct bandgaps of monolayers and the potential difference of water splitting (1.23 eV), respectively. The E denotes the photon energy utilized for water splitting determined by:

$$E = \begin{cases} E_g, (\chi(H_2) \geq 0.2, (\chi(O_2) \geq 0.6) \\ E_g + 0.2 - \chi(H_2), (\chi(H_2) < 0.2, (\chi(O_2) \geq 0.6) \\ E_g + 0.6 - \chi(O_2), (\chi(H_2) \geq 0.2, (\chi(O_2) < 0.6) \\ E_g + 0.8 - \chi(H_2) - \chi(O_2), (\chi(H_2) < 0.2, (\chi(O_2) < 0.6) \end{cases} \tag{S4}$$

Among them, $\chi(H_2)$ and $\chi(O_2)$ represent the overpotential of hydrogen evolution reaction (HER) and oxygen evolution reaction (OER) respectively. The intrinsic electric field does positive work for the electron−hole separation during the process of photocatalytic water splitting. Therefore, this part of work should be added into the total energy, and then the corrected STH efficiency of photocatalytic water splitting for 2D material with intrinsic vertical electric field is calculated as:

$$\eta_{STH}{}^{c} = \eta_{STH} \times \frac{\int_{0}^{\infty} P(\mathrm{h}\omega) d(\mathrm{h}\omega)}{\int_{0}^{\infty} P(\mathrm{h}\omega) d(\mathrm{h}\omega) + \Delta\Phi \int_{E_g}^{\infty} \frac{P(\mathrm{h}\omega)}{\mathrm{h}\omega} d(\mathrm{h}\omega)} \tag{S5}$$

where $\Delta\Phi$ is the vacuum level difference on the two respective surfaces of the Si_4HX monolayers, and the second term in the denominator represents the work done by the intrinsic vertical electric field. In addition, the $\Delta\Phi$ difference between the initial and final states of the Si_4HX monolayers is very small, and its influence on the hydrogen production efficiency can be ignored. Here, the band gaps, $\chi(H_2)$, and $\chi(O_2)$ predicted by HSE06 function are used to calculate these energy conversion efficiencies.

Piezoelectricity refers to the polarization generated in an asymmetric structure when external stress or electric field is applied to the structure,[3] as well as the linear part of the coupling effect between the dielectric and elastic properties of the crystal. The piezoelectric

stress tensor e_{ijk} and the piezoelectric strain tensor d_{ijk} follow the relationship:[4]

$$e_{ijk} = \frac{\partial P_i}{\partial \varepsilon_{jk}} = \frac{\partial \sigma_{jk}}{\partial E_i} \tag{S6}$$

$$d_{ijk} = \frac{\partial P_i}{\partial \sigma_{jk}} = \frac{\partial \varepsilon_{jk}}{\partial E_i} \tag{S7}$$

where P_i, ε_{jk}, σ_{jk} and E_i represent the polarization, stress tensor, strain tensor and electric field, respectively. The subscript *i, j* and *k* each can present the *x*, *y* or *z*-direction. For simplicity, the three-order tensor d_{ijk} and e_{ijk} are usually replaced by d_{ik} (3×6 matrix) and e_{il} (3×6 matrix). The new defined subscript *i* can be set as 1, 2 and 3, which corresponds to the *x*, *y* and *z*-direction, respectively. *l* represents the second-order tensor *xx*, *yy*, *zz*, *yz*, *zx* and *xy*, which are represented by numbers 1, 2, 3, 4, 5 and 6, respectively. d_{ik} and e_{il} have the following relationship:[5]

$$e_{il} = d_{ik} C_{kl} \tag{S8}$$

the four-order tensor C_{kl} (6×6 matrix) is the elastic stiffness coefficient. For these Si_4HX monolayers with C_{3v} symmetry, the e_{il} and C_{kl} can be expressed as:[5, 6]

$$e_{il} = \begin{pmatrix} 0 & 0 & 0 & 0 & e_{15} & e_{16} \\ -e_{22} & e_{22} & 0 & e_{15} & 0 & 0 \\ e_{31} & e_{31} & e_{33} & 0 & 0 & 0 \end{pmatrix} \tag{S9}$$

$$C_{kl} = \begin{pmatrix} C_{11} & C_{12} & C_{13} & C_{14} & 0 & 0 \\ C_{12} & C_{11} & C_{13} & -C_{14} & 0 & 0 \\ C_{13} & C_{13} & C_{33} & 0 & 0 & 0 \\ C_{14} & -C_{14} & 0 & C_{44} & 0 & 0 \\ 0 & 0 & 0 & 0 & C_{44} & C_{14} \\ 0 & 0 & 0 & 0 & C_{14} & 0.5\left(C_{11} - C_{12}\right) \end{pmatrix} \tag{S10}$$

Therefore, the d_{ik} matrix can be derived as:

$$d_{ik} = \begin{pmatrix} 0 & 0 & 0 & 0 & d_{15} & d_{16} \\ -d_{22} & d_{22} & 0 & d_{15} & 0 & 0 \\ d_{13} & d_{31} & d_{33} & 0 & 0 & 0 \end{pmatrix} \tag{S11}$$

In this paper, we focus on the e_{31} and d_{31}, the relationship between them is described by the following formula:[7]

$$d_{31} = \frac{e_{31}}{C_{11} + C_{12}} \tag{S12}$$

The out-of-plane piezoelectricity of 2D materials refers to the phenomenon that the polarized charges generated on the surface of 2D materials perpendicular to the plane of 2D materials after applying stress or strain to the material. The out-of-plane stress and strain

piezoelectric coefficients (e_{31} and d_{31}) are corresponding to the polarization along the *z*-direction. This is because 2D materials possess a large surface area, and those with excellent out-of-plane piezoelectric properties can generate a substantial amount of polarization charges on the material surface under external stress, making them more favorable for practical applications.

The expressed as:[5]

$$Z_{ij}^{*} = \frac{S}{|e|}\frac{\partial P_i}{\partial u_j^I} \tag{S13}$$

where S is the surface area of the unit cell of 2D material, e is the elementary charge, P_i is the dipole moment per unit area, and u_j^I is the displacement of ion I in the j direction under the action of stress along the i direction ($i = j = x, y, z$). The piezoelectricity of a material, i.e., the rate of change of polarization of the material under external stress, corresponds exactly to the overall effect of the Born effective charges (BECs) of each atom. Therefore, the BECs of each atom in the material can effectively reflect the piezoelectricity of the material.[5, 8-10]

The applicability of materials to electronic devices depends greatly on their transport properties, especially carrier mobility. Here, we investigate the transport characteristics of Si_4HX monolayers based on their orthorhombic cells. The deformation potential approximation is one of the most common methods to calculate the mobility of carriers.[11] The mobility of carriers for the 2D structures can be calculated as follows:[12]

$$\mu = \frac{e\hbar^3 C_{2D}}{k_B T m^* \bar{m} E_d^2} \tag{S14}$$

where e is the elementary charge, C_{2D} stands for the in-plane stiffness, E_d refers to the deformation potential constant, k_B and $\hbar$ are, respectively, the Boltzmann constant and the reduced Planck constant, m^* and $\bar{m} = \sqrt{m_x m_y}$ stand for the effective mass and the average effective mass of carriers, and T = 300 K is the temperature used in these calculations.

The effective mass of the carriers represents their ability to respond to the external field and directly affects their mobility. The effective masses of electron (m_e^*) and hole (m_h^*) can be obtained by fitting the parabolic function to the band edges (conduction band minimum (CBM) and valence band maximum (VBM)) via the expression:

$$\frac{1}{m} = \frac{1}{\hbar^2}\left|\frac{\partial^2 E(k)}{\partial k^2}\right| \tag{S15}$$

where $E(k)$ is the wave-vector k-dependence of energy at the CBM/VBM (in the $k_x k_y$ plane). The characteristics of the carrier transport are investigated along two different directions in the reciprocal-lattice space. From Eq. S15, we can see that the flatter the energy structure around the band edges is, the larger are the carrier effective masses. This is because the larger the radius of curvature, the smaller the second derivative $\partial^2 E(k)/\partial k^2$. The C_{2D} for 2D materials is evaluated by the following formula:

$$C_{2D} = \frac{1}{S_0}\frac{\partial^2 E}{\partial \varepsilon_{uni}^2} \quad \text{(S16)}$$

where E is the total energy, ε_{uni} refers to the uniaxial strain along the two transport directions x and y, and S_0 is the area of the optimized unit cell. The deformation potential constant E_d can be expressed as:

$$E_d = \frac{\Delta E_{edge}}{\varepsilon_{uni}} \quad \text{(S17)}$$

where E_{edge} stands for the energy shifting of the band edges with respect to the vacuum level. The positions of band edges (CBM and VBM) and energy shifting are investigated within the uniaxial strain range from -0.5% to 0.5% along the two transport directions x and y. By fitting the strain-dependent energy and band energies of the VBM and CBM with respect to the vacuum energy, we can obtain the elastic modulus and deformation potential constant.[12, 13] The calculated results for the above physical quantities of the Si_4HX monolayers are listed in Table S3.

Table S3 The carrier effective mass $|m_{x/y}|$ (m_0), deformation potential constant $|E_{d,x/y}|$ (eV), and elastic stiffness coefficients $|C_{2D,x/y}|$ (N/m) of the Si_4HX monolayers.

Monolayer	Carrier type	$\|C_{2D,x}\|$	$\|C_{2D,y}\|$	$\|m_x\|$	$\|m_y\|$	$\|E_{d,x}\|$	$\|E_{d,y}\|$
Si_4HF_{IS}	Light hole	110.31	111.16	0.41	0.40	2.62	3.89
	Heavy hole			1.44	2.30		
	Electron			0.25	2.64	2.41	2.13
Si_4HF_{FS}	Light hole	112.79	114.48	0.39	0.36	1.99	2.49
	Heavy hole			1.21	1.61		
	Electron			0.24	2.84	2.23	1.67
Si_4HCl_{IS}	Light hole	113.65	113.24	0.42	0.37	3.23	4.55
	Heavy hole			1.50	2.67		
	Electron			0.25	2.64	4.89	2.78
Si_4HCl_{FS}	Light hole	114.07	114.01	0.41	0.37	3.01	3.99
	Heavy hole			1.26	1.75		
	Electron			0.24	2.92	2.71	1.32
Si_4HBr_{IS}	Light hole	115.95	116.31	0.44	0.39	3.97	4.46
	Heavy hole			1.68	2.95		
	Electron			0.25	2.65	3.01	2.31
Si_4HBr_{FS}	Light hole	119.26	119.48	0.42	0.39	3.29	3.43
	Heavy hole			1.39	2.35		
	Electron			0.24	2.85	2.73	1.99

Table S4 The vacuum level on the lower/upper side E_{vac1}/ E_{vac2}, the band edges with respect to the vacuum level $E_{\mathrm{CBM/VBM}}{}^{vac}$, the Over-Potential for Hydrogen Evolution Reaction $\chi(H_2)$, and the Over-Potential for Oxygen Evolution Reaction $\chi(O_2)$ of the Si_4HX monolayers (in units of eV) under the HSE06 level at pH = 0. The adsorption energies of the water molecule in top side/bottom side E_{vac1}/ E_{vac2} of the Si_4HX monolayers (in units of eV).

Material	Si_4HF_{IS}	Si_4HF_{FS}	Si_4HCl_{IS}	Si_4HCl_{FS}	Si_4HBr_{IS}	Si_4HBr_{FS}
E_{vac1}	3.55	3.62	3.43	3.35	3.23	3.23
E_{vac2}	1.29	1.35	2.22	2.15	2.33	2.34
$E_{\mathrm{CBM}}{}^{vac}$	-3.26	-3.29	-3.27	-3.34	-3.30	-3.38
$E_{\mathrm{VBM}}{}^{vac}$	-7.44	-7.28	-6.41	-6.26	-6.07	-5.93
$\chi(H_2)$	1.18	1.15	1.17	1.10	1.14	1.06
$\chi(O_2)$	1.77	1.61	0.74	0.59	0.40	0.26
E_{ads1}	-0.28	-0.17	-0.25	-0.17	-0.26	-0.25
E_{ads2}	-0.29	-0.26	-0.27	-0.27	-0.29	-0.29

The change of Gibbs free energy (ΔG) in water splitting reaction is calculated using the method proposed by Nørskovet et *al.*[14] The formula can be expressed as:

$$\Delta G = \Delta E + \Delta E_{ZPE} - T\Delta S \tag{S18}$$

where ΔE represents the energy changes of reaction intermediates in the free state and the adsorbed state, ΔE_{ZPE} and ΔS are the differences in the zero-point energy and entropy difference between the adsorbed state and corresponding free-standing state, respectively.

E_{ZPE} could be derived after the frequency calculation by

$$E_{ZPE} = 1/2 \sum h\nu \tag{S19}$$

where ν represents the vibrational frequency.

Meanwhile, *TS* is given by

$$TS = k_b T\left[\sum_K In(\frac{1}{1-e^{-h\nu/k_bT}}) + \sum_K \frac{h\nu}{k_bT}(\frac{1}{e^{-h\nu/k_bT}-1}+1)\right] \tag{S20}$$

where *e* represents the electron charge, *h* represents Planck's constant and k_b is Boltzmann's constant. Here, T is set to be 298.15K.

The effect of external potential and pH have been taken into account to evaluate the

HER and OER activities. The ΔG for HER process include two steps, which was expressed as:

$$* + \mathrm{H^+} + \mathrm{e^-} \rightarrow \mathrm{H^*} \quad \text{(S21)}$$

$$\Delta G_1 = G_{H*} - \frac{1}{2} G_{H_2} - G_* + \Delta G_U - \Delta G_{PH} \quad \text{(S22)}$$

$$\mathrm{H^*} + \mathrm{H^+} + \mathrm{e^-} \rightarrow * + \mathrm{H_2(g)} \quad \text{(S23)}$$

$$\Delta G_2 = G_* + \frac{1}{2} G_{H_2} - G_{H*} + \Delta G_U - \Delta G_{PH} \quad \text{(S24)}$$

Meanwhile, the OER can be decomposed into four elementary steps. The ΔG for each step was calculated as follows:

$$\mathrm{H_2O(l)} + * \rightarrow \mathrm{OH^*} + \mathrm{H^+} + \mathrm{e^-} \quad \text{(S25)}$$

$$\Delta G_3 = G_{OH*} + \frac{1}{2} G_{H_2} - G_* - G_{H_2O} + \Delta G_U - \Delta G_{PH} \quad \text{(S26)}$$

$$\mathrm{OH^*} \rightarrow \mathrm{O^*} + \mathrm{H^+} + \mathrm{e^-} \quad \text{(S27)}$$

$$\Delta G_4 = G_{O*} + \frac{1}{2} G_{H_2} - G_{OH*} - G_{H_2O} + \Delta G_U - \Delta G_{PH} \quad \text{(S28)}$$

$$\mathrm{H_2O(l)} + \mathrm{O*} \rightarrow \mathrm{OOH^*} + \mathrm{H^+} + \mathrm{e^-} \quad \text{(S29)}$$

$$\Delta G_5 = G_{OOH*} + \frac{1}{2} G_{H_2} - G_{O*} - G_{H_2O} + \Delta G_U - \Delta G_{PH} \quad \text{(S30)}$$

$$\mathrm{OOH^*} \rightarrow * + \mathrm{O_2(g)} + \mathrm{H^+} + \mathrm{e^-} \quad \text{(S31)}$$

$$\Delta G_6 = G_* + \frac{1}{2} G_{H_2} + G_{O_2} - G_{OOH^*} + \Delta G_U - \Delta G_{PH} \quad \text{(S32)}$$

where ΔG_U ($\Delta G_U = -eU$) denotes extra potential bias provided by an electron in the electrode, where U represents the potential difference from the standard hydrogen electrode potential. ΔG_{pH} represents the effect of pH on ΔG, which is calculated by $\Delta G_{pH} = k_b T \times ln10 \times$ pH.

Table S5 Carrier mobilities μ ($cm^2\ V^{-1}\ s^{-1}$) for electron (e) and hole (h) along x- and y-directions, energy conversion efficiencies of light absorption η_{abs} (%), carrier utilizations η_{cu} (%), solar-to-hydrogen (STH) efficiencies η_{STH} (%), corrected STH η_{STH}^{c} (%), the total piezoelectric stress coefficients e_{31} (in units of 10^{-10} C / m), and the built-in electric field E_{int} (in units of 10^9 V/m) of some 2D semiconductors in previous works at 300 K and pH = 0.

Monolayer	μ_e^x	μ_h^x	μ_e^y	μ_h^y	η_{abs}	η_{cu}	η_{STH}	η_{STH}^{c}	e_{31}	E_{int}	Ref
Si_4HF_{IS}	2.00×10^3	2.07×10^3	0.24×10^3	0.67×10^3	61.14	48.83	29.86	24.68	0.323	-3.23	This work
Si_4HF_{FS}	2.45×10^3	4.17×10^3	0.37×10^3	2.93×10^3	70.48	52.22	36.81	28.86	0.329	-3.23	
Si_4HCl_{IS}	0.50×10^3	1.41×10^3	0.15×10^3	0.80×10^3	60.57	48.64	29.46	26.53	0.094	-1.62	
Si_4HCl_{FS}	1.63×10^3	1.69×10^3	0.65×10^3	1.06×10^3	70.48	51.70	36.44	31.81	0.093	-1.62	
Si_4HBr_{IS}	1.34×10^3	0.86×10^3	0.22×10^3	1.06×10^3	63.44	37.57	23.83	21.88	0.013	-1.18	
Si_4HBr_{FS}	1.72×10^3	1.39×10^3	0.27×10^3	1.38×10^3	73.15	33.92	24.81	22.23	0.016	-1.16	
MoSSe	52.72	0.21×10^3	65.82	0.25×10^3	– –	– –	– –	– –	– –	1.90	15, 16
MoSeTe	37.25	0.10×10^3	36.43	0.11×10^3	– –	– –	– –	– –	– –	– –	
MoSTe	77.83	24.00	78.53	23.33	– –	– –	– –	– –	– –	– –	
WSSe	0.13×10^3	0.72×10^3	0.12×10^3	0.43×10^3	30.72	41.26	12.67	11.68	– –	– –	17
PtSSe	2.58×10^3	31.00	0.14×10^3	20.00	31.3	59.5	18.6	17.7	– –	– –	18
Al_2S_3	0.61×10^3	0.40×10^3	1.93×10^3	0.34×10^3	7.2	37.8	2.7	2.6	– –	– –	2
Al_2Se_3	1.58×10^3	0.56×10^3	1.20×10^3	0.51×10^3	20.9	43.6	9.1	8.0	– –	– –	
Al_2Te_3	5.10×10^3	0.31×10^3	0.71×10^3	0.42×10^3	61.1	46.6	28.4	21.4	– –	– –	
Zn_2SSe	2.17×10^3	0.24×10^3	2.16×10^3	0.39×10^3	7.94	38.19	3.03	3.01	– –	– –	19
Zn_2STe	0.99×10^3	86.00	2.99×10^3	0.19×10^3	71.82	23.75	17.05	16.28	– –	– –	

Zn_2SeTe	1.82×10^3	0.10×10^3	2.05×10^3	0.13×10^3	57.69	28.48	16.43	16.43	– –	– –	
Al_2CClBr	0.84×10^3	62.86	0.52×10^3	52.32	– –	– –	– –	5.26	– –	– –	20
$AlScCCl_2$	1.32×10^3	97.36	8.27×10^3	0.32×10^3	– –	– –	– –	13.04	– –	– –	
$AlScCBr_2$	4.64×10^3	0.14×10^3	11.82×10^3	0.13×10^3	– –	– –	– –	15.58	– –	– –	
AlScCBrCl	24.60×10^3	57.57	8.88×10^3	34.45	– –	– –	– –	12.94	– –	– –	
$NbOCl_2$[a]	62.01	28.97	0.25×10^3	0.23	37.73	37.39	14.11	– –	– –	– –	21
$NbOBr_2$	0.11×10^3	46.06	0.52×10^3	10.79	40.85	39.99	16.34	– –	– –	– –	
$AgBiP_2Se_6$	– –	– –	– –	– –	23.12	44.40	10.27	10.04	– –	– –	
$AgBiP_2S_6$	– –	– –	– –	– –	2.78	34.56	0.96	0.96	– –	– –	22
$CuBiP_2Se_6$	– –	– –	– –	– –	27.58	30.15	8.32	8.06	– –	– –	
$CuBiP_2S_6$	– –	– –	– –	– –	10.78	39.62	4.27	4.21	– –	– –	
ZrSSe	– –	– –	– –	– –	– –	– –	– –	– –	0.005	– –	
ZrSeTe	– –	– –	– –	– –	– –	– –	– –	– –	-0.115	– –	
ZrSTe	– –	– –	– –	– –	– –	– –	– –	– –	0.003	– –	9
HfSSe	– –	– –	– –	– –	– –	– –	– –	– –	0.048	– –	
HfSTe	– –	– –	– –	– –	– –	– –	– –	– –	0.129	– –	
$MoSiGeN_4$	– –	– –	– –	– –	– –	– –	– –	– –	– –	2.74	23

[a] Band structure of $NbOCl_2$ monolayer was applied with 1% tensile strain.

The optimized POSCAR data of Si_4HX monolayers are as follows:

Si_4HF_{IS}
1.000000
3.8755168617543081 -0.0000000000275802 -0.0000000000000001
-1.9377584309765645 3.3562960550477521 0.0000000000000002
-0.0000000000000005 0.0000000000000004 30.0000000000000000
F H Si
1 1 4
Cartesian
-0.0000019637155224 2.2375317702994084 5.1254471036206710
1.9377603358843625 1.1187641842699709 12.1278514545549427
-0.0000019637155225 2.2375317702994084 6.7521916192110183
-0.0000000000000001 0.0000000000000001 7.5036097139521285
1.9377603358843625 1.1187641842699707 10.6245197976347612
-0.0000000000000001 0.0000000000000001 9.8674936461896161

Si_4HF_{FS}
1.00000000000000
3.8688674059006392 0.0000000000000000 0.0000000000000000
-1.9344337029004062 3.3505374573490307 0.0000000000000000
0.0000000000000000 0.0000000000000000 30.0000000000000000
F H Si
1 1 4
Direct
0.6666669843821182 0.3333329855491556 0.1703528233311391
0.6666669843821182 0.3333329855491556 0.4047721109351768
0.6666669843821182 0.3333329855491556 0.2245603690418717
-0.0000000000000000 -0.0000000000000000 0.2498346865609253
0.6666669843821182 0.3333329855491556 0.3546723522332446
-0.0000000000000000 0.0000000000000000 0.3291780946309735

Si_4HCl_{IS}
1.00000000000000
3.8723626719761310 -0.0000000000004951 0.0000000000000000
-1.9361813359384836 3.3535644465428351 0.0000000000000000
-0.0000000000000005 0.0000000000000000 30.2207907466325452
H Si Cl
1 4 1
Direct
0.6666669844098223 0.3333329855815705 0.3993947910490832
0.3333329857889495 0.6666669846230633 0.2209141595755852
0.0000000000000000 0.0000000000000000 0.2463409754868522
0.6666669844098223 0.3333329855815705 0.3496448376156920

0.0000000000000000 0.0000000000000000 0.3245338867342085
0.3333329857889495 0.6666669846230633 0.1523899422086075

Si_4HCl_{FS}

1.00000000000000

3.8653048894343840 0.0000000000162931 0.0000000000000000
-1.9326524447530367 3.3474522275989420 -0.0000000000000000
0.0000000000000001 0.0000000000000000 30.0553252538409517

H Si Cl
1 4 1

Direct
0.6666669845801962 0.3333329857373570 0.4084734635604725
0.6666669845801962 0.3333329857373570 0.2280120073223035
0.0000000000000000 0.0000000000000000 0.2538006616009320
0.6666669845801962 0.3333329857373570 0.3584646622406957
0.0000000000000000 0.0000000000000000 0.3329675355908013
0.6666669845801962 0.3333329857373570 0.1591533687847781

Si_4HBr_{IS}

1.00000000000000

3.8817540409294318 0.0000000000001920 0.0000000000000000
-1.9408770204144288 3.3616976106581187 0.0000000000000000
0.0000000000000002 0.0000000000000000 30.4551676668358908

H Si Br
1 4 1

Direct
0.6666669845904352 0.3333329857330298 0.3989694871806577
0.3333329855330334 0.6666669844181285 0.2221173299695991
0.0000000000000000 0.0000000000000000 0.2471598901695415
0.6666669845904352 0.3333329857330298 0.3495948926087351
0.0000000000000000 0.0000000000000000 0.3247884990863810
0.3333329855330334 0.6666669844181285 0.1485885304278725

Si_4HBr_{FS}

1.00000000000000

3.8747239531371243 0.0000000000000551 0.0000000000000000
-1.9373619765183925 3.3556093760797752 0.0000000000000000
-0.0000000000000001 0.0000000000000000 29.9033260677420749

H Si Br
1 4 1

Direct
0.6666669845233741 0.3333329856659404 0.4087428003394464
0.6666669845233741 0.3333329856659404 0.2275956263309098
0.0000000000000000 0.0000000000000000 0.2533335799785448

0.6666669845233741	0.3333329856659404	0.3584741150314699
0.0000000000000000	0.0000000000000000	0.3329640675555936
0.6666669845233741	0.3333329856659404	0.1527611515202381

References

[1] T. A. Manz, *Rsc Advances*, 2017, **7**, 45552-45581.

[2] C.-F. Fu, J. Sun, Q. Luo, X. Li, W. Hu and J. Yang, *Nano Letters*, 2018, **18**, 6312-6317.

[3] S.-E. Park and T. R. Shrout, *Journal of Applied Physics*, 1997, **82**, 1804-1811.

[4] L. Dong, J. Lou and V. B. Shenoy, *ACS Nano*, 2017, **11**, 8242-8248.

[5] P. Nandi, A. Rawat, R. Ahammed, N. Jena and A. De Sarkar, *Nanoscale*, 2021, **13**, 5460-5478.

[6] D. Dimple, N. Jena, A. Rawat, R. Ahammed, M. K. Mohanta and A. De Sarkar, *Journal of Materials Chemistry A*, 2018, **6**, 24885-24898.

[7] H.-N. Zhang, Y. Wu, C. Yang, L.-H. Zhu and X.-C. Wang, *Physical Review B*, 2021, **104**, 235437.

[8] M. Noor-A-Alam, O. Z. Olszewski and M. Nolan, *Acs Applied Materials & Interfaces*, 2019, **11**, 20482-20490.

[9] Dimple, N. Jena, A. Rawat, R. Ahammed, M. K. Mohanta and A. De Sarkar, *Journal of Materials Chemistry A*, 2018, **6**, 24885-24898.

[10] M. Li, O. Omisakin and J. Young, *Nanoscale*, 2022, **14**, 6970-6980.

[11] N. N. Hieu, H. V. Phuc, A. I. Kartamyshev and T. V. Vu, *Physical Review B*, 2022, **105**, 075402.

[12] W. Wan, S. Zhao, Y. Ge and Y. Liu, *Journal of Physics: Condensed Matter*, 2019, **31**, 435501.

[13] S.-D. Guo, W.-Q. Mu, Y.-T. Zhu, R.-Y. Han and W.-C. Ren, *Journal of Materials Chemistry C*, 2021, **9**, 2464-2473.

[14] J. K. Nørskov, J. Rossmeisl, A. Logadottir, L. Lindqvist, J. R. Kitchin, T. Bligaard and H. Jónsson, *The Journal of Physical Chemistry B*, 2004, **108**, 17886-17892.

[15] C. Xia, W. Xiong, J. Du, T. Wang, Y. Peng and J. Li, *Physical Review B*, 2018, **98**, 165424.

[16] J. Min, G. Guo, M. Zhou, T. Zhang, M. Liu and Y. Deng, *Physics Letters A*, 2024, **494**, 129283.

[17] L. Ju, M. Bie, X. Tang, J. Shang and L. Kou, *ACS Applied Materials & Interfaces*, 2020, **12**, 29335-29343.

[18] P. Jamdagni, A. Kumar, S. Srivastava, R. Pandey and K. Tankeshwar, *Physical Chemistry Chemical Physics*, 2022, **24**, 22289-22297.

[19] X. Tan, Q. Chen, Y. Liang, Z. Tian, T. Gao and Q. Xie, *International Journal of Hydrogen Energy*, 2024, **51**, 222-230.

[20] Y.-X. Du, Y. Mu, W.-M. Liu, X. Jia, J.-H. Lin and T. Zhang, *Applied Surface Science*, 2025, **702**, 163289.

[21] L. Pan, Y.-L. Wan, Z.-Q. Wang, H.-Y. Geng and X.-R. Chen, *Journal of Applied Physics*, 2023, **134**, 085105.

[22] L. Ju, J. Shang, X. Tang and L. Kou, *Journal of the American Chemical Society*, 2020, **142**, 1492-1500.
[23] M.-M. Dong, C.-K. Wang, X.-X. Fu and M.-W. Zhao, *Journal of Materials Science & Technology*, 2025,